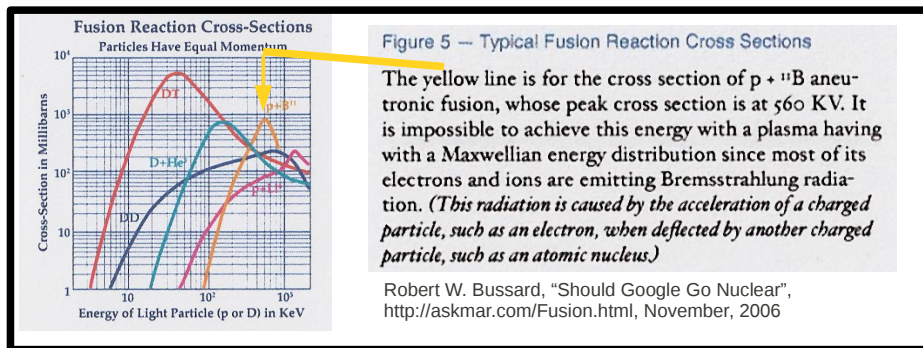# A "Polywell" p+^{11}B Power Reactor

Joel G. Rogers, Ph.D.

rogersjg@telus.net

Aneutronic fusion is the holy grail of fusion power research. A new method of operating Polywell was developed which maintains a non-Maxwellian plasma energy distribution. The method extracts down-scattered electrons and replaces them with electrons of a unique higher energy. The confined electrons create a stable electrostatic potential well which accelerates and confines ions at the optimum fusion energy, shown in the graph below. Particle-in-cell(PIC) simulations proceeded in two steps; 1) operational parameters were varied to maximize power balance(Q) in a small-scale steady-state reactor; and 2) the small scale simulation results were scaled up to predict how big a reactor would need to be to generate net power. Q was simulated as the ratio of fusion-power-output to drive-power-input. Fusion-power was computed from simulated ion density and ion velocity. Power-input was simulated as the power required to balance non-fusing ion losses. The predicted break-even reactor size was 13m diameter. Bremsstrahlung losses were also simulated and found manageable.
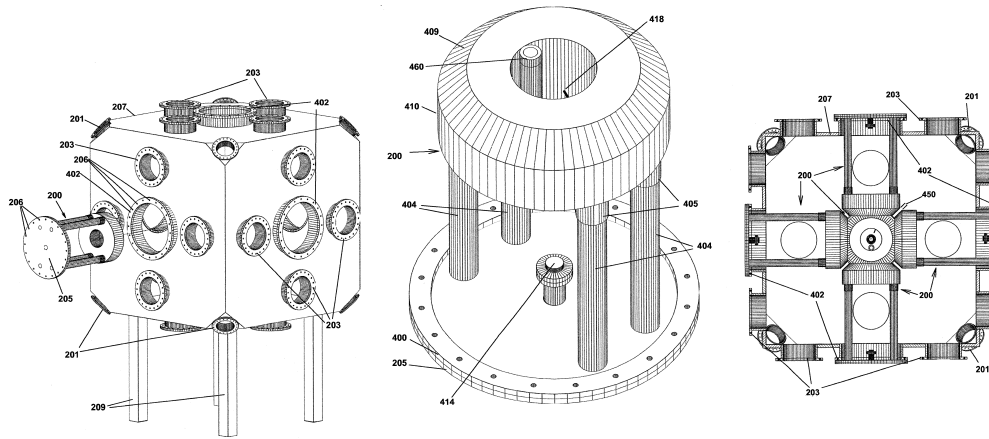
Fusion Reaction Cross-Sections
Particles Have Equal Momentum

Figure 5 --- Typical Fusion Reaction Cross Sections

The yellow line is for the cross section of p + ^{11}B aneu-tronic fusion, whose peak cross section is at 560 KV. It is impossible to achieve this energy with a plasma having with a Maxwellian energy distribution since most of its electrons and ions are emitting Bremsstrahlung radia-tion. (*This radiation is caused by the acceleration of a charged particle, such as an electron, when deflected by another charged particle, such as an atomic nucleus*)

Robert W. Bussard, "Should Google Go Nuclear", http://askmar.com/Fusion.html, November, 2006

These 15 slides were presented on December 8, 2011 at the 13th U.S.- Japan Workshop on Inertial Electrostatic Confinement Fusion (http://www.physics.usyd.edu.au/~khachan/IEC2011/Presentations/Rogers.pdf)

Repeating the abstract:
"Aneutronic fusion is the holy grail of fusion power research. A new method of operating Polywell was developed which maintains a non-Maxwellian plasma energy distribution. The method extracts down-scattered electrons and replaces them with electrons of a unique higher energy. The confined electrons create a stable electrostatic potential well which accelerates and confines ions at the optimum fusion energy, shown in the graph [above]. Particle-in-cell(PIC) simulations proceeded in two steps; 1) operational parameters were varied to maximize power balance(Q) in a small-scale steady-state reactor; and 2) the small scale simulation results were scaled up to predict how big a reactor would need to be to generate net power. Q was simulated as the ratio of fusion-power-output to drive-power-input. Fusion-power was computed from simulated ion density and ion velocity. Power-input was simulated as the power required to balance non-fusing ion losses. The predicted break-even reactor size was 13m diameter. Bremsstrahlung losses were also simulated and found manageable."

Fig. 2 - "Polywell" Patent Pending

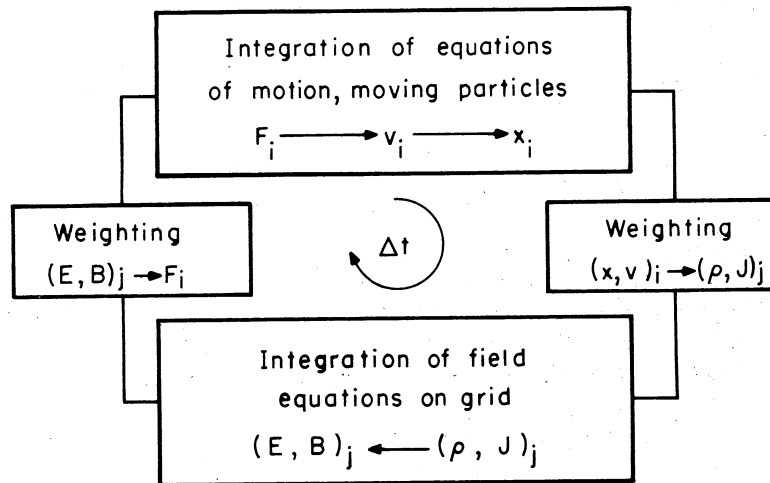U.S. Patent Application "Modular Apparatus for Confining a Plasma", filed 2008

The above drawings are from the author's 2008 patent application, published 2010 and available on the U.S. patent office website, http://appft.uspto.gov/netahtml/PTO/search-bool.html, as Publication Number 20100284501. The author's patent application improves on an earlier (2006) patent application of Robert W. Bussard, published 2011 as Publication Number 20110170647. The Bussard patent is still pending, awaiting a decision by the patent office Board of Appeals. The author's patent incorporates for the first time independent supports of the magnet coils by horizontal and vertical legs. The placement of the legs was designed by computer simulation to allow free recirculation of electrons in and out of the central region. Free recirculation of electrons reduces the drive power input requirement to a practical level and should allow for the first time constructing a net power reactor.

The left-hand drawing above shows a cubic vacuum tank with six 14"-flange openings for mounting six identical magnet modules, one of which is shown expanded in the central drawing. The right-hand drawing shows a two-dimensional(2D) central section of the proposed reactor, which was simulated in 2D PIC formalism using a commercial software package. The electrical components shown are the grounded vacuum tank(207), four floating electron emitters(414) and insulating hollow legs(404), grounded at the outer end and at biased at the inner end. The legs support coil-magnet boxes(410), four of which are shown enclosing a square central area where the ion plasma is confined. Magnet boxes were biased to high voltage 400kV which attracted electrons from the emitters into the central enclosure. The magnets are arranged to have the magnetic field of all magnets pointing inward toward the center. This arrangement guides electrons from the emitters into the central volume and forces them to circulate in and out of the central volume along magnetic-field cusp lines. Electrons circulate through the centers of the coils and through narrow gaps(450) between chamfered surfaces(409) of the adjacent magnet enclosures. Eight ion guns, one of which is shown(460), inject proton and boron ions into the central enclosure. The magnets confine the electrons and the electrons confine the ions long enough for fusion to take place.

The 4 electron emitters shown serve a dual purpose in the simulation. They emit electrons to replace those that are lost by hitting internal structures and they also intercept and remove down-scattered electrons. The size and placement of the emitters was chosen to stabilize the average energy of the electrons using an arbitrarily selected electron current of 50A per electron gun.

The present status of these two pending patent applications can be retrieved using the patent office PAIR system (http://portal.uspto.gov/external/portal/pair) to access the patents' "Image File Wrapper" with the above Publication Numbers.

Fig. 3 - PIC Simulation Flowchart

Figure 2-3a A typical cycle, one time step, in a particle simulation program. The particles are numbered $i = 1, 2, \ldots,$ NP; the grid indices are j, which become vectors in 2 and 3 dimensions.
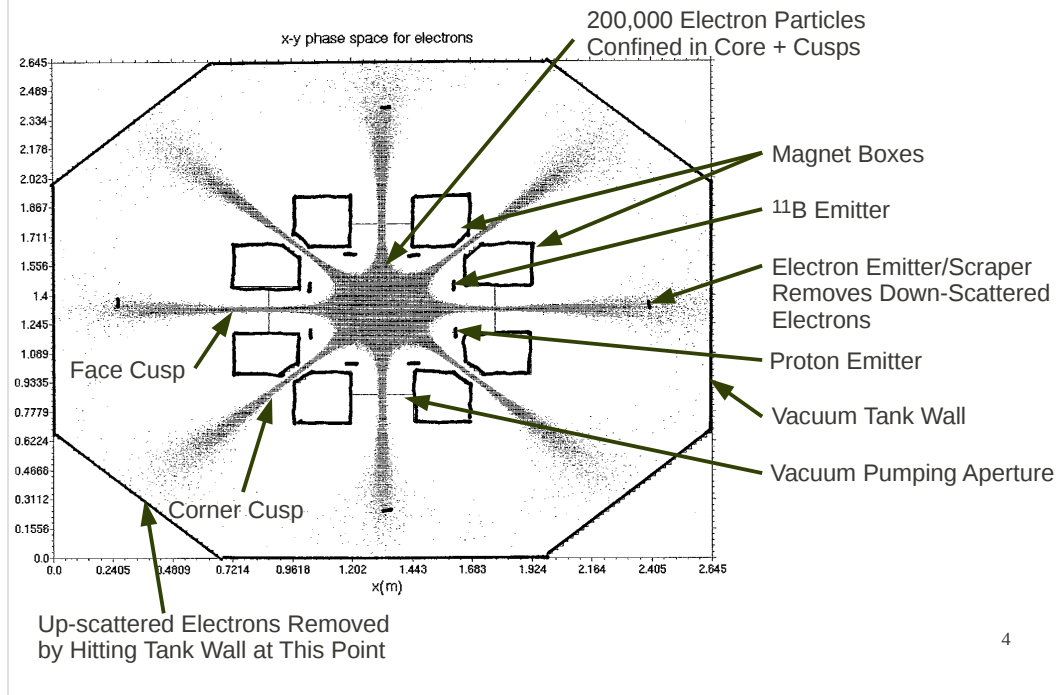
The Figure and caption were scanned from the textbook by Charles K. Birdsall and A. Bruce Langdon, "Plasma Physics via Computer Simulation", McGraw Hill, New York, 1985, pg. 11.

In simulation a two-dimensional slab of plasma was represented as an array of 128x128 cells, indexed by "j" in the above flowchart. Time advances step by step in increments of Δt, 10 picoseconds. At steady-state 300,000 electron and ion particles, indexed by "i" in the flowchart, were tracked in time and space as they moved under the influence of the Lorentz force. At each time-step the program executes a loop by performing the 4 operations in the boxes in sequence, starting on the left. The left box uses the fields in each cell to calculate the Lorentz force on each particle; the top box moves particles from cell to cell; the right box calculates particle densities and currents; and the bottom box calculates each cell's magnetic(B) and electric(E) fields. At start-up time(t=0) the simulation contained cells and fields but no particles, simulating an empty vacuum tank. As time went on electrons formed a potential well and newborn ions were accelerated to fusion velocity by the Coulomb force, derived from the potential. At the end of the start-up phase of simulation, electron and ion source rates were empirically reduced to smaller values, chosen to stabilize the densities.

Hardware dimensions, voltages, magnetic fields, and source particle currents were specified by a 1000 line input file in the source language of the OOPIC simulation software package. A public version of OOPIC, called XOOPIC, is distributed free by the U.C. Berkeley Electrical Engineering and Computer Sciences Department (http://www.eecs.berkeley.edu/IPRO/Software/Description/oopic.html). For this work an equivalent commercial version, called OOPIC-Pro, was purchased from Tech-X Corporation of Colorado (txcorp.com).

Fig. 4 - Electrons' 2D Positions

x-y phase space for electrons

200,000 Electron Particles
Confined in Core + Cusps

Magnet Boxes

^{11}B Emitter

Electron Emitter/Scraper
Removes Down-Scattered
Electrons

Proton Emitter

Vacuum Tank Wall

Vacuum Pumping Aperture

Face Cusp

Corner Cusp

Up-scattered Electrons Removed
by Hitting Tank Wall at This Point

4

This snapshot of a 2D diagnostic plot was made at a time once the simulation reached steady-state conditions. Each electron particle is shown as a black dot and hardware components are identified by arrows. In the on-line version of this diagnostic the dots move with each time-step. This plot, and similar ones for protons and boron ions, provided an on-line monitor of the functioning of the simulation program. Initially, at time equal zero, there were no dots showing. As time went on dots originated at the positions of 4 electron emitters and accelerated into the core under the influence of the attractive 400kV bias on the magnet boxes. The combined effect of the electrons' momentum and the applied magnetic and electric fields cause most of the electrons to fly through the core and exit the magnets' enclosure along one of 8 cusp lines. Electrons re-circulate out and in many times until they eventually scatter and hit something.

Protons and boron ions originated at 4 proton guns and 4 boron guns inside the magnet enclosure, indicated by arrows. For simplicity, the ions were created fully stripped, i.e. borons all had charge 5e.The proton guns and the boron guns were positioned all at the same distance from the center. This choice caused the newborn protons and borons to fall through the same E-field by the same distance which made the boron particle energy 5 times the proton particle energy.
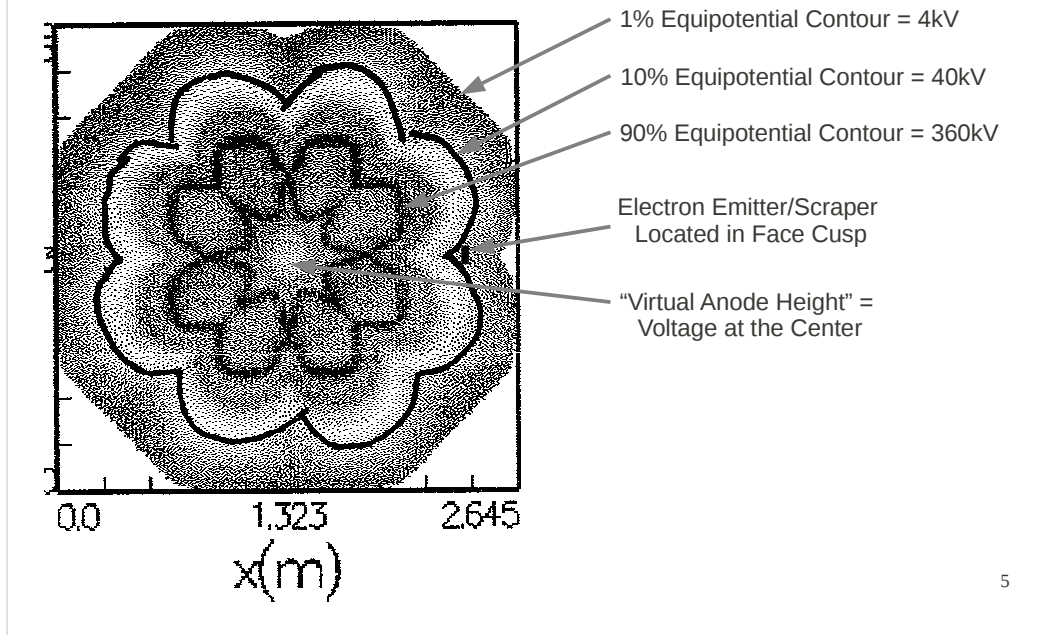
During steady-state operation, up-scattered electrons escape along one of the cusp lines and hit the tank walls. Each lost electron is replaced by a newborn electron from the electron emitters, maintaining fixed electrical charge. This replacement mechanism resets the deviant velocities of up-scattered electrons, but not down-scattered electrons. Bussard proposed "annealing" as a mechanism to correct down-scattered electrons. In reference [1] below Bussard wrote the following:

> "The important feature is the balance between up- and down-scattering in a single pass of an electron through the system. If the up-scattering in core region passage is removed by the down-scattering in [exterior] collisions with cold ions, then the core electron energy will be stable."

The annealing mechanism described by Bussard has NOT been observed in these scale model simulations. As the ion density rose during startup, the potential well became shallower and shallower, causing a cooling of the ions below the fusion energy. The failure of annealing created the need for a new method to correct down-scattered electrons and thereby obtain stability.

[1] Bussard, Robert W., King, Katherine E., "Bremsstrahlung Radiation Losses in Polywell Systems," 1991, EMC2-0891-04, http://askmar.com/Fusion.html

Fig. 5 - Confining Electrostatic Potential

1% Equipotential Contour = 4kV

10% Equipotential Contour = 40kV

90% Equipotential Contour = 360kV

Electron Emitter/Scraper
Located in Face Cusp

"Virtual Anode Height" =
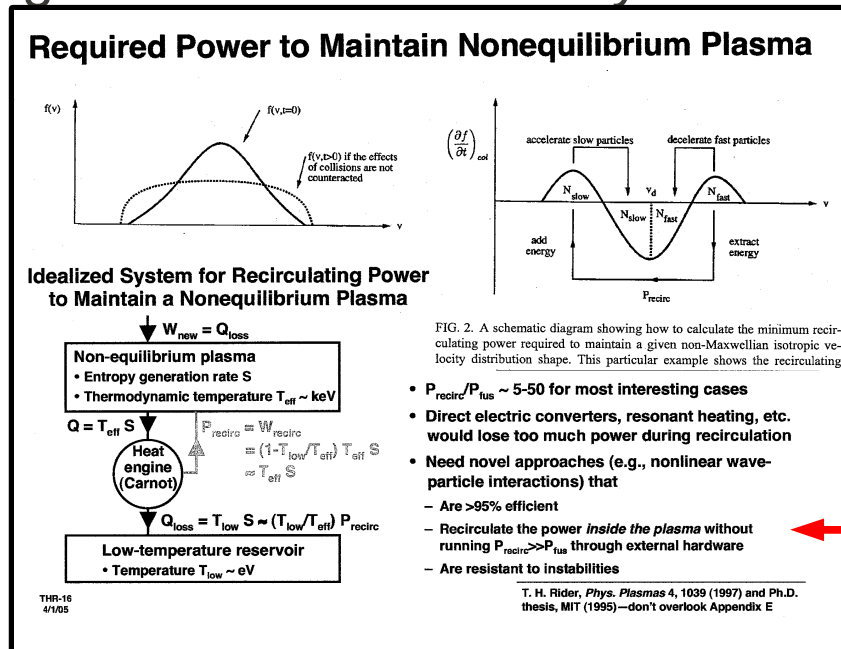Voltage at the Center

The 2D map above is a diagnostic generated by the simulation program which shows the electrostatic potential function. The maximum of the potential is in the darkest shaded regions, labeled "90% Equipotential Contour", which surround the magnet boxes. A hand-drawn contour, labeled "10% Equipotential Contour," was added to show the shape of the field outside the magnets. The shape of the potential function is such that it attracts electrons outside the core and attracts ions inside the core. The value of the potential at the center of the core is what Bussard[1] called the "virtual anode height." Here the light shading indicates a virtual anode height about 20% of the maximum voltage, 400kV, which occurs in the cusps midway through the magnet coils.

Born from emitters outside the magnets' enclosure, incoming electrons reach their maximum velocity midway through the center of a magnet coil. Momentum carries them inside the well where they slow down as they approach the repulsive core. Most electrons bounce off the core and exit through a corner cusp adjacent to the face cusp they came in on. Momentum carries these electrons outward through the magnets. Outside they are decelerated by the bias voltage. Their velocity falls to zero as they approach the tank wall; they turn around near the tank wall and fall back through the same cusp opening where they came out. The electron's second and subsequent cycles repeat the first cycle with minor variations caused by scattering. Typically each electron recycles many times in and out along adjacent cusp lines. Eventually an electron gains or looses energy by scattering on electrons and ions. Some electrons up-scatter and some electrons down-scatter. Up-scattered electrons end their lives hitting the tank wall at the end of one of the 8 cusp lines. Down-scattered electrons end their lives hitting one of the electron emitters, using a new method to be described.

Also in ref. [1] Bussard states that effective annealing requires a small virtual anode height, on the order of 1% of the electron drive energy. A small anode height is desirable but has not been obtainable in the present simulation, even with testing a wide range of operating parameters (e.g. electron/ion drive currents and source positions). To obtain stability, i.e. densities and velocities constant in time, it was necessary to introduce a new method of correcting the down-scattered electrons back to the energy they had when they were originally injected from the electron emitters.

[1] Bussard, Robert W., King, Katherine E., "Bremsstrahlung Radiation Losses in Polywell Systems," 1991, EMC2-0891-04, http://askmar.com/Fusion.html
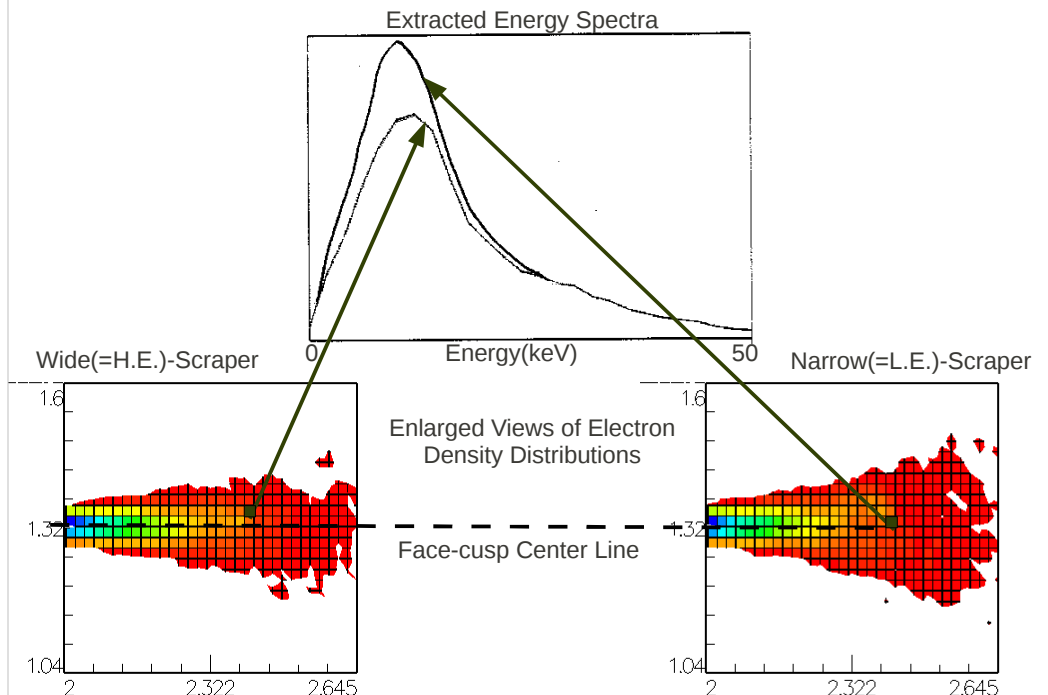
The Figure shows a stylized copy of a slide shown by Todd H. Rider in 2005 as part of a 26-slide presentation entitled "Is There a Better Route to Fusion?". A link to Rider's pdf file is currently available on the website of the Longwood University Physics Department under student project "Farnsworth Fusion Reactor" (longwood.edu/chemphys/7677.htm). Rider's earlier work, referenced at the bottom of the Figure, concluded that external energy recirculation, e.g. a Carnot heat engine, was too inefficient to maintain the narrow electron velocity spread required for Polywell. In this 2005 "publication" Rider suggested a possible work-around for his earlier dire prediction. As shown by the red arrow (◀━) above, IEC reactors might work if they "recirculate the power inside the plasma," thereby avoiding the Carnot inefficiency.

Bussard's proposed annealing mechanism would recirculate electron power inside the plasma, if it worked. Unfortunately annealing has not been observed in the small scale model simulation described here. As a slightly less efficient alternative to annealing, the present simulation describes removal of up-scattered electrons at the 8 intersection points where the cusp lines meet the tank walls.

Up-scattered electrons give up most of their kinetic energy to the electrostatic potential which slows them on their way to hitting the wall. Although they have energy 400keV inside the core, they have only about 10 keV when they reach the wall. For each lost electron a fresh electron is generated by the electron emitters. The vast majority of the lost electron's original kinetic energy is transferred via the potential and with perfect efficiency to the newborn electron that replaces it. The inefficiency of the Carnot heat engine only applies to the small fraction of recirculated energy still carried by the electron when it hits the wall.

Down-scattered electrons are more of a challenge to recycle. They turn back along the cusp lines before reaching the tank walls. If not corrected by some other means, they would accumulate in the cusps and destroy the potential well needed to accelerate/confine the ions. To remove/reset down-scattered electrons a new method was implemented as described in the next slide.

Fig. 7 - Scraping Down-Scattered e's

Extracted Energy Spectra

Wide(=H.E.)-Scraper

Narrow(=L.E.)-Scraper

Energy(keV)

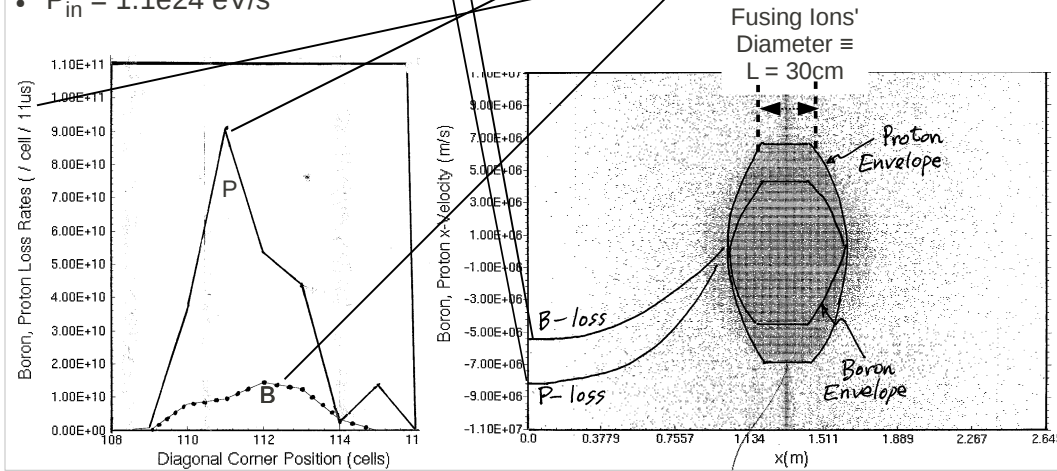Enlarged Views of Electron Density Distributions

Face-cusp Center Line

This slide illustrates a method of recycling/resetting down-scattered electrons' energies. The method utilizes a feature of the electron population in the outer portions of the face cusps. The electron energy is dispersed by the external magnetic field near the face cusps' axes. Higher energy electrons tend to transport themselves across the magnetic field to greater distances off-axis than lower energy electrons. Lower energy electrons tend to stay closer to the cusp axis along which they exited the core. This feature of the transport allows the lower energy electrons to be "scraped" off by a physical barrier located close to the face cusp axis and extending out only a short distance from the axis. More of the higher energy (un-scattered) electrons pass by the barrier and return to the core.

In the lower portion of the Figure are steady-state snapshots of 2D electron density made with two different placements of the scraper electrodes; except for the scraper positions these diagnostics were simulated with identical reactor conditions. The range of the x- and y-coordinates in the snapshots cover only a small portion of the area inside the tank, namely the electron distribution immediately adjacent to the "Electron Emitter/Scraper..." label in Fig. 4. The physical extent of the scraper is shown as a small black square occupying one cell of the simulation volume. Upward pointing arrows connect the two scraper positions with energy spectra made from the electrons which were extracted on the scrapers during steady-state running. The energy spectrum from the scraper placed closer to the axis is peaked at a lower energy than the spectrum made with the scraper placed further from the axis. This difference in energy spectra confirms that the scraper position selects the energy of the extracted electrons; lower energy electrons will be selected by a scraper placed closer to the axis. The remainder of the simulations in this report were made with all four electron emitters placed in the low-energy(L.E.) position, i.e. as close as possible to the face cusp axes. Such a placement is shown for a typical one of the emitters in the Figure and labeled "Narrow(=L.E.)-Scrapper."

Unfortunately, the placement of the scrapers cannot be claimed to be optimum. The face cusps in the 2D simulation are necessarily represented as line cusps, whereas the real 3D world face cusps would be point cusps. Because of this lack of reality in the simulation, the electron losses in the simulation are excessive compared to the real world. To correct for this, electron losses were ignored in favor of the more realistic simulation of ion losses. By this approximation we assume that eventual optimization with a 3D model will actually show that real electron losses are small enough to warrant ignoring them compared to the ion losses. This is a reasonable assumption in that the magnet bias prevents electrons from returning to their birth position which is spaced well inside the tank wall. Only up-scattered electrons can reach the tank walls and these up-scattered electrons are exactly the ones we most want to extract and replace.

Fig. 8 - Ion Loss Power Calculation

- P_{in} ≡ proton energy-loss-rate + boron energy-loss-rate (through corner cusps)

  = (# slabs/cube) (# cusps/slab) {Σ[Particle Loss-energy)][Particle loss-rate]}

  = (L/λ_D) (4) {[½(956MeV)(8e6)²/c²][½(114-110)(9e10)/(11e-6s)]

  　　+[½(11)(931MeV)(5.4e6)²/c²][½(114-110)(1.2e10)]/[(11e-6s)]}

  = (30)(4){[(340keV)(1.6e16/s)]+[(1700keV)(2.2e15/s)]} = 6.5e23 + 4.5e23

- P_{in} = 1.1e24 eV/s

This Figure shows the formula and the diagnostic plots used in computing Pin, the denominator of the power balance Q. Ignoring the ions lost through the face cusps and also ignoring the power lost to recycling electrons, Pin was approximated as the ions' loss rate through the corner cusps only. An imaginary real-world cubic reactor was modeled as a stack of identical slabs of plasma. The simulated power loss from one slab was multiplied by the number of slabs which would stack up to make a cubic volume of fast ions. The slab thickness was taken to be the Debye length λ_D of the electron plasma.

The two diagnostic plots below the formula for Pin determine the factors in the formula. The first factor, the number of slabs per cube, is the height of the fusing plasma cube divided by the slab thickness λ_D, The height "L" was determined from the right-hand diagnostic plot, a snapshot of ion particle positions, each ion represented as a black dot in x-velocity vs. x-position phase-space. During their lifetime trapped in the well, protons and boron ions circulate in two overlapping elliptical regions in phase-space, shown enclosed by the hand-drawn curves labeled "Proton-Envelope" and "Boron-Envelope." The cross section for fusion is strongly peaked toward the extreme velocities of the proton and boron ions in the appropriate regions. For the purpose of computing Q, the x-, y-, and z- dimensions of the plasma cube were taken to be equal to L; as indicated in the right hand diagnostic, L includes only the high-velocity ions.

The 2nd factor, number of cusps per slab, scales up the losses on one corner-segment, simulated to save time. From symmetry, the losses on the other 3 corners of the slab would be the same, hence the factor of 4.

The {3rd factor} is the sum(Σ) of the proton plus boron power loss for one slab. Each of the two species of charged ions take away power equal to the lost particle current times the lost particle's kinetic energy expressed in volts. The hand-traced curves in the left-hand diagnostic plot show the number of lost particles on one corner segment of the tank. These numbers were converted to particle currents by computing the area under the curves and then dividing by the time duration of the simulation, 11 microseconds for this run. The area was approximated as a triangle, of which the (114-110) factor is the base width measured in units of cells. The hand-drawn curves labeled "B-loss" and "P-loss" trace streams of up-scattered borons and protons moving toward the left tank-wall, shown at x=0. Once an up-scattered ion leaves the magnet enclosure it experiences an electric field accelerating it toward its death at the tank wall. The ions' have a unique x-velocity at the wall, read from the points where the curves meet the ordinate scale. Velocities were converted to energies via the usual kinetic energy = ½MU² expression, embedded in {3rd factor}.

Fig. 9 - Power Balance Q

- Simulated (R = 35cm) power balance: $Q(R) \equiv P_{fus} / P_{in}$ where:

  - $P_{fus} = n_p n_b <\sigma_f v> L^3 E_f$ eV/s (from Glasstone and Lovberg eq. 2.10 [2])

    - n_p = proton 3D density $\equiv N_p / \lambda_D$ = 1.1e17/m3
    - n_b = boron 3D density = n_p / Z (Proton and boron partial pressures are made equal.)
    - Z = boron charge state from ion gun = 5
    - N_p = simulated (2D) proton density = 1.1e15/m2 (Fig. 10)
    - λ_D = Debye length = $7.43e2 \, E_e^{1/2} n_e^{-1/2}$ cm = 0.01m (Fig.10 & Formulary pg. 28 [3])
    - E_e = maximum electron energy inside well = 400keV (Fig. 10)
    - $n_e = 2n_p$ (Plasma quasi-neutrality is an inherent property of the simulation.)
    - <> = fusion x.c. times c.m. velocity = 8e-29m2 x 1e7m/s = 8e-22m3/s (Title page)
    - L = ion plasma cube dimension in meters = 0.3m (from previous slide)
    - E_f = fusing ion pair energy release in eV = 8.7 MeV (Formulary pg. 44 [3])

  - P_{fus} = (1.1e17) (2.2e16) (8e-22) (0.3³) (8.7e6) eV/s = 4.5e17 eV/s

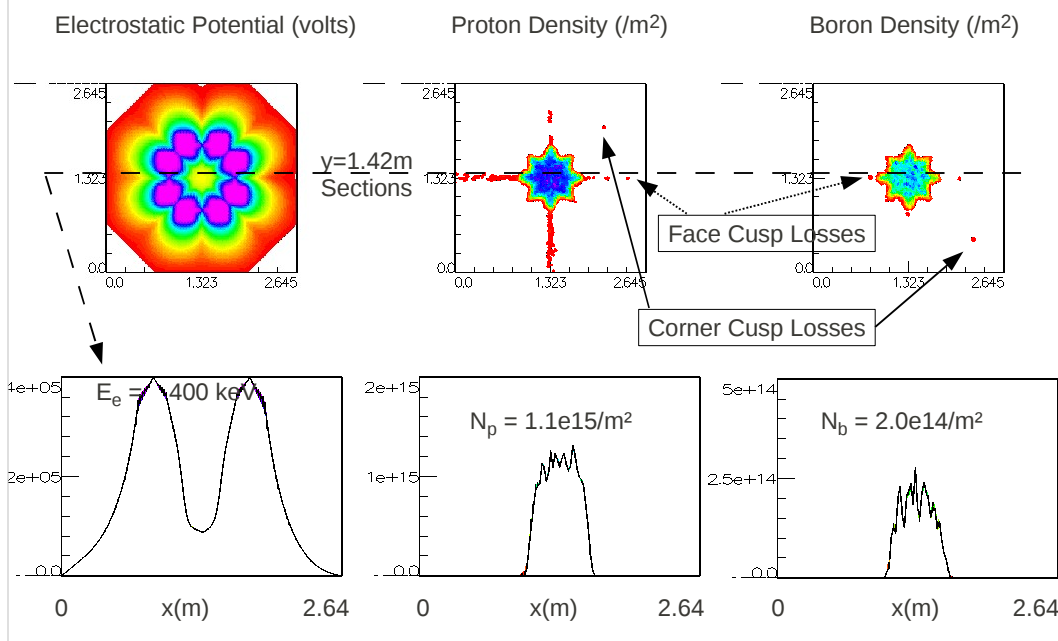- Q(R=35cm) = P_{fus} / P_{in} = 4.5e17 / 1.1e24 = 4.1e-7 (P_{in} from Fig. 8)

[2] Glasstone and Lovberg, "Controlled Thermonuclear Reactions", van Nostrand, 1960
[3] Formulary, wwwppd.nrl.navy.mil/nrlformulary/NRL_FORMULARY_11.pdf

9

The first line in the Figure is the standard formula for power balance Q. The numerator of Q is the fusion power output at steady-state, Pfus, given by the formula in the second line; it depends on the simulated proton and boron densities, velocities, and volume of the plasma cube, L^3. Proton and boron densities were independently controlled in the simulation by specifying the currents from the proton and boron ion guns. The relative ion velocity, v in the formula, is the sum of the proton and boron velocities, which are themselves determined by the depth of the potential, the positions of the guns inside the well and the charge of the ions falling into the well. The positions of the ion guns were chosen to be as far inward from the inner surface of the magnets as possible without impeding the flow of the circulating electrons.

To reduce the complexity of searching for optimum values of the many parameters determining the reactor operating point, additional simplifying assumptions were made relating the parameters. One important parameter of the plasma is the ratio of thermal to magnetic energy density at the plasma surface, known as Beta. The particle densities were fixed to make the Beta value of ions and electrons approximately equal to each other. When the Beta values were varied to approach unity, the cusp losses increased. To avoid excessive losses, Beta was selected to be somewhat less than unity. Electron Beta was calculated using the expression $\beta = 4.03e-11 \, n_e E_e / B^2$, from pg. 29 of the NRL Plasma Formulary (ref. [3] above). Using density and energy the same as used in computing λ_D above, and B = 3.5kG measured in the corner cusps, electron Beta was calculated to be 0.29. In extrapolating the size of the model reactor to net-power size, electron Beta and ion Beta were assumed to stay constant as the hypothetical reactor size increased. Fixing β and E_e makes n_e proportional to B^2 and therefore $n_p n_b$ proportional to B^4.

The simulated B field was the sum of fields from 4 coils arranged in a square. The ratio of the electrical current to magnetic field was scaled up from published current specification of a 1.75kW water-cooled copper coil magnet available from GMW Associates (gmw.com). The simulation shown above used a scale factor of 2, which produced a magnet radius of R = 35cm. A second simulation, shown in Fig. 11, utilized a scale factor of 3 which produced a magnet radius of R = 52cm. The overall size of the net-power reactor depends on our choice of magnet technology. Cryogenic cooling might someday reduce the size of the magnets and therefore the size of the net-power reactor. The present choice of copper magnets is a conservative engineering choice considering the magnets must withstand a substantial heat load from bremsstrahlung which must be disposed of along with the magnets' resistive heat load.

Fig. 10 - Diagnostics Determining P_{fus}

Electrostatic Potential (volts)   **Proton Density (/m²)**   **Boron Density (/m²)**

y=1.42m Sections

Face Cusp Losses

Corner Cusp Losses

$E_e = 400\ keV$

$N_p = 1.1e15/m^2$

$N_b = 2.0e14/m^2$

x(m)   x(m)   x(m)

The square plot in the upper left of the Figure is a 2D map of the electrostatic potential inside the tank. The 8 squarish regions arranged in a circle are the outlines of 8 magnet boxes, modeled as metal conductors and biased to 400kV. The maximum potential occurs at the surfaces of and inside the magnet boxes. The dashed arrow through the plot marks a 1D section selected to pass close to the inner surfaces of two magnet boxes. The 1D potential along this line is shown in the lower left plot. The potential reaches a maximum of 400kV at two point along this line. The electron energy at these points, Ee = 400keV, was used in computing the electrons' Debye length and Beta in the previous slide. Ions experience the same potential as the electrons. Ions initially fall into the well between the two peaks, then circulate back and forth through the center until they either fuse or hit some internal structure.

The two 2D plots at center and on the right show the 2D density distributions of proton and boron ions. One-dimensional(1D) sections were made along the same horizontal line as for the potential. The values of the central densities for protons and borons, called Np and Nb, were read from these plots and inserted into the formula for Pfus in the previous slide.

The 2D density plots illustrate the ions' loss mechanism. Arrows point to red blobs which represent individual proton and boron particles which have escaped the core along one of the cusp lines. The simulation shows that face cusps(dashed arrows) leak more ions than corner cusps(solid arrows), but this is a fake. In the simulation both face cusps and corner cusps necessarily have the shape of line cusps. The simulated face cusps leak more than the corner cusps because the B-field is weaker in the faces than in the corners. In the real world, corner cusps leak more than face cusps, the opposite of the simulation. This feature of real world Polywell was emphasized by Bussard in paragraph [0211] of his abandoned patent application (reference [4] below), where he wrote the following:
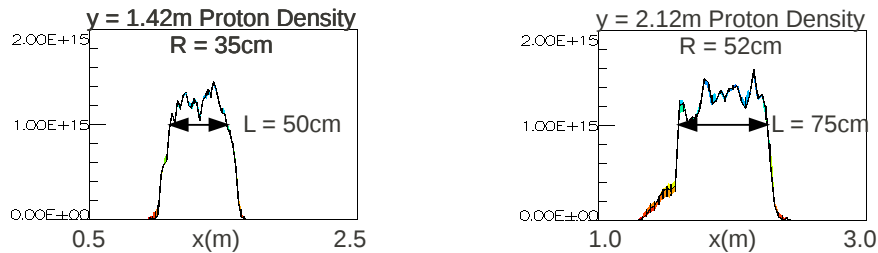
> "circulation through the semi-line-cusps at the spaced corners [allows] much greater throughflow per unit area than through the point cusps of the polyhedral faces".

To compensate for the simulation's over-estimate of face cusp losses, only the corner cusp losses were included in the calculated power loss, Pin. After escaping through a corner cusp the ion particles, typical ones of which are shown above, are observed to be moving along diagonal lines and impact a diagonal corner segment of the vacuum tank; there they were counted in a diagnostic plot separately from those ions exiting through face cusps.

[4] Robert W. Bussard, "Method and apparatus for controlling charged particles", U.S. Patent Appl. Doc. No. 20080187086.

Fig. 11 - Reactor Break-Even Radius

- Bussard's Scaling Formula: $Q_1/Q_2 = (R_1/R_2)^5$

- Break-Even Formula: $Q(R=35cm)/Q(R_b) = (R/R_b)^5$

  - $Q(R_b) \equiv 1$

- Solving for Break-Even Radius: $R_b = R/Q^{1/5}$

- $R_b = 0.35m/(4.1e{-}7)^{0.2} = 6.6m =$ smaller than **ITER**

y = 1.42m Proton Density
R = 35cm
L = 50cm
2.00E+15 · 1.00E+15 · 0.00E+00
0.5   x(m)   2.5

y = 2.12m Proton Density
R = 52cm
L = 75cm
2.00E+15 · 1.00E+15 · 0.00E+00
1.0   x(m)   3.0

11

Bussard claims empirical evidence for his 5th power scaling formula in paragraph [0124] of his pending patent application (reference [5] below). Examining the form of the expression for Q (= Pfus / Pin), we see the only parameters that depend on magnet size are $n_p n_b$, L, and P_{in}. Holding Beta constant makes $n_p n_b$ scale as R^4, as shown in Fig. 9. To investigate the scaling of L, a second simulation was done with a magnet radius 1.5x larger, namely R = 52cm. The diagnostic plots in the above Figure compare proton ion densities for the two magnet sizes. The width of the density distribution on the right is 1.5 times the width of the distribution on the left, showing that L scales linearly with R, as Bussard predicted. Combining this R^3 scaling of plasma volume with the R^4 scaling of $n_p n_b$, we find Pfus scales as the 7th power of R.

The remaining factor determining the scaling of Q is its denominator, Pin. Bussard stated in paragraph [0124] of ref. [5] that Pin scales as R^2, but he did not provide any details or references backing up this statement. His reasoning might have been the following: For line cusps, the cusp area is the product of the line's dimension perpendicular to the simulated plasma slab times its width parallel to the slab. In the perpendicular direction the dimension would be the height of the cubic reactor, which is proportional to R. In the parallel direction the cusp dimension would be the ion gyroradius, which is inversely proportional to B (Formulary[3] pg. 28) and therefore inversely proportional to R. Multiplying the height by the width to get the area of the cusp makes the area independent of R. The remaining factor in Pin should be the ion thermal pressure at the cusp. This pressure factor is proportional to the ion density, which scales quadratically with R. Combining these factors, Pin is proportional to a constant cusp area times the ion density, which is to say Pin scales as R^2.

Combining the scaling of numerator and denominator, Q scales as the ratio $R^7/R^2 = R^5$. By this line of reasoning we have "proved" Bussard's scaling formula, $Q1/Q2 = (R1/R2)^5$.

This scaling leads to a predicted break-even magnet radius Rb = 6.6m, about half the size of ITER. Using the 7th power scaling of Pfus, the net power output of a "Polywell" reactor the **same size as ITER** would be 2^7 times more power than the break-even reactor output evaluated in the Figure above. This power would be $P(R=13m) = (1.6e{-}19)(4.5e17)(6.6/0.35)^7(2^7)$ Watts = 7.6 Gigawatts. A reactor of this size and power output would be useful in land-based power stations, but might be too big for transportation applications.

[5] Robert W. Bussard, "Method and apparatus for controlling charged particles", U.S. Patent Appl. Doc. No. 20110170647

Fig. 12 - Bremsstrahlung Power Loss

- $P_b = 1.69\text{e-}32\ n_e\ T_e^{1/2}\ [n_p + Z^2 n_b]\ L^3$ (Watts)

- $P_b = 1.1\text{e-}13\ n_e^2\ T_e^{1/2}\ [0.5 + (25)(0.1)]\ L^3$ (eV/s)

  - n_e = electron density in cm^{-3} = 2.2e11/cm^3 (Fig. 9)

  - T_e = electron kinetic energy in eV = 80keV (Fig 13)

  - L = electron core edge dimension in cm = 30cm (Fig. 13)

- $P_b = 1.1\text{e-}13\ (2.2\text{e}11)^2\ (8\text{e}4)^{1/2}\ [3.0]\ (30)^3$ eV/s

- $P_b = 1.3\text{e}17$ eV/s

- $P_b \approx 30\%\ P_{fus}$ (Fig. 9)

- Bremsstrahlung losses ≈ 1/3 fusion output power

12

The first line above gives the formula for bremsstrahlung from Glasstone and Lovberg[7], Chapter 2. Their derivation of the formula assumes Maxwellian distribution of electron velocities, and might therefore seem questionable for our non-Maxwellian electrons. However, close examination of the derivation of the formula in their section 2.63 reveals that the assumption of Maxwellian distribution is only needed to express Pb in units of temperature. We only need Pb in terms of electron energy Te; for this the Glasstone and Lovberg derivation is equally valid for our approximately monoenergetic velocity distribution as for their Maxwellian.
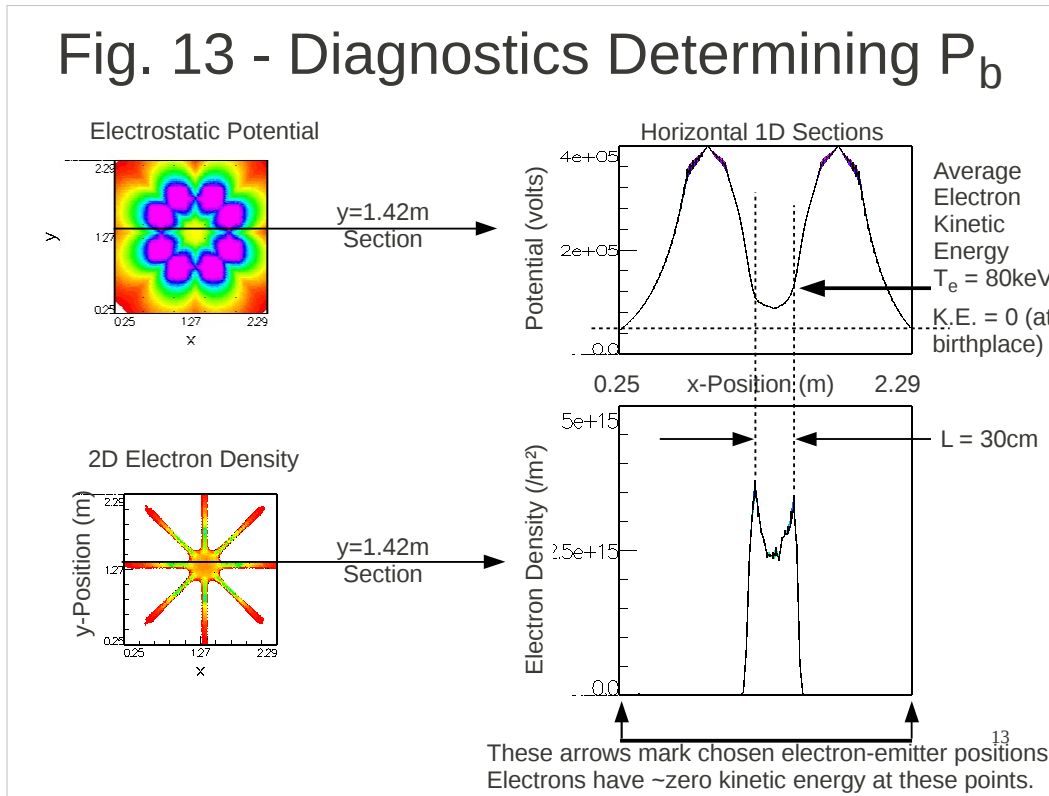
Radiative power loss increases with density in the same proportion as Q, so its importance does not scale away with reactor size like the ion losses do. Radiated power cannot be efficiently recovered to supplement drive power because the radiated x-rays hit the magnets and are there converted to heat which must be disposed of by existing magnet cooling. The above formula shows radiated power Pb is proportional to the square-root of the central electron kinetic energy which is approximately equal to Bussard's "virtual anode height". As shown in the next Figure, our model design produced Te = 80keV, about 20% of the incoming electron energy. This is much greater than the 1% virtual anode height Bussard said is needed for annealing, as discussed in Fig. 5.

Another important factor in Pb is the boron density n_b. Because its contribution is multiplied by the square of the boron charge, it dominates over the radiation from the proton density(n_p) factor. In the present design the boron density is 1/5 the proton density, chosen to equalize the thermal pressure of the two components. Even with this relatively small boron percentage, the radiated boron-electron power is 5 times bigger than the proton-electron power.

A third important factor in Pb is the volume of electrons confined in the central region, L^3. Surprisingly this volume is the same as the ions' volume factor used in computing Q in Fig. 8-9. Although the ions' total volume exceeds the electrons' volume, only the central fast ions were included in the dimension L because the slow outer ions don't fuse due to the falloff of cross section with velocity. The volume of **radiating** electrons is the same as the volume of **fusing** ions, approximated as the volume of a cube of dimension L.

The above calculation shows that the scale model will exhibit a 30% loss of power due to bremsstrahlung. This percentage loss will persist at larger radii and might become increasingly troublesome as the reactor size grows above net power. Radiative power lost to the magnets will burden the cryogenic cooling system of the magnets, needed to reduce their resistive losses. Designing a reactor with smaller central electron energy Te is an ongoing quest of the simulation.

Fig. 13 - Diagnostics Determining P_b

Electrostatic Potential

Horizontal 1D Sections

y=1.42m Section

Potential (volts)

4e+05

2e+05

0.0

Average Electron Kinetic Energy T_e = 80keV

K.E. = 0 (at birthplace)

0.25   x-Position (m)   2.29

2D Electron Density

y-Position (m)

y=1.42m Section

Electron Density (/m²)

5e+15

2.5e+15

0.0

L = 30cm

These arrows mark chosen electron-emitter positions. Electrons have ~zero kinetic energy at these points.

The two parameters that most effect the bremsstrahlung power loss are the central electron kinetic energy, parametrized byTe, and the volume of the cubic electron cloud, parametrized by L. Electrons move in a potential well, shown in the top panels of this Figure. The left panel shows a 2D representation and the right hand panel shows a 1D section made at the position of the right-going arrow. The electrons' kinetic energy along this 1D section is the difference in potential energy between the electron's birthplace, indicated by the dashed line, and its average position, indicated by the left-pointing arrow. This energy difference varies from 40 to 80keV over the central region where the ions live. The radiative power loss, Pb in the previous Figure, is proportional to the square-root of the "average" energy, symbolized by Te.

The size of the radiating electron volume, L, was determined from the diagnostics in the lower half of the Figure. The 2D electron density function on the left was sectioned at the same position as the potential above. The right-going arrow shows this section of the 2D density in units of electrons per square meter. The electrons' density distribution is narrower than the corresponding ion distributions(Fig. 10) and peaked at the surface of the electron cloud, indicated by the vertical dashed lines. Because of this peaking, most of the bremsstrahlung radiation originates near the surface of the electron cloud. For the purpose of computing Pb, the value of Te was defined to be the electrons' kinetic energy at the surface, as marked by the intersection of the vertical dashed lines with the potential function in the top-right panel.

The desired estimate of radiative power loss could be more accurately computed as a spatial integral of the power density, expressing electron density, ion density and electron energy as appropriate functions of 2D position. The evaluation of Pb described above is a convenient approximation made by replacing the desired spatial integral by the product of most probable electron energy times the approximate volume of radiating electrons.

To minimize radiative losses it is important to make Te as small as possible. The 80keV shown was the smallest attainable by searching over the machine parameters in the simulation; however the search was not exhaustive. Further reduction of Te may be possible as discussed in the next Figure.

Fig. 14 - How to Reduce P_b Losses

- $P_b \sim T_e^{\frac{1}{2}} \, [1 + 25 \, (n_b/n_p) \,]$

- To reduce P_b the reactor design can change:
  - Reducing T_e to 1% E_e would reduce P_b by 4.5X. (ref. [1])
  - Reducing n_b/n_p from 1/5 to 1/10 would reduce P_b by 2X.

- Reducing T_e might increase reactor size R_b.
  - Not yet tested in simulation.

- By both these measures taken together:
  - Radiation might be reduced to 5% of fusion power.

14

Both T_e and n_b/n_p can be reduced by adjusting the parameters defining the reactor design. In the present simulation, adjusting Te downward could be accomplished by decreasing the plasma density. However this would have the side effect of increasing the break even reactor size, Rb. A larger reactor size might be acceptable, considering the substantial power-to-size advantage the present design has over ITER.

What level of bremsstrahlung radiation loss is acceptable can be related to the efficiency of the conversion of fusion power to electrical power. Conversion efficiency will be in the range 30-70%, depending on whether steam generators or direct electrical converters are employed. Adjusting only the boron fraction n_b/n_p, the radiation loss might be reduced to 15% of the fusion output, less than the power lost to conversion inefficiency. Even the existing design's radiation loss of 30% might be considered acceptable since it is no worse than the essential inefficiency of conversion..

By these estimates it appears that bremsstrahlung power loss will a manageable problem in "Polywell" p+B11 reactors.

An extensive discussion of the measures which can be used to further reduce radiative losses can be found in ref. [1] and ref. [7] below.

[1] Bussard, Robert W., King, Katherine E., "Bremmstrahlung Radiation Losses in Polywell Systems," 1991, EMC2-0891-04, http://askmar.com/Fusion.html

[7] Bussard, Robert W., King, Katherine E., "Bremsstrahlung and Synchrotron Radiation Losses in Polywell Systems," 1991, EMC2-1291-02, http://askmar.com/Fusion.html

Fig. 15 - p + ^{11}B Power; Conclusions

- New method efficiently recycles electron energy.
- Simulation predicts break-even R_b = 6.6m
- Additional design issues still need attention:
  - Electron power drain must be reduced.
  - Bremsstrahlung power drain must be reduced.
- A 3D simulation is needed for more realistic P_{in}.
- The future of aneutronic fusion power is bright.

This simulation of a p+boron reactor predicts a much improved break-even radius Rb compared to last year's simulation of D+D reactor, reported in ref. [8] below. The improvement in Rb is mainly due to a different set of assumptions regarding the relative importance of electron and ion losses. Last year the electron losses were assumed to dominate the losses. This year the electron losses were ignored on the theoretical grounds that electron confinement is a more manageable problem which will be solved by future design improvements. This assumption must be tested by ongoing simulations. Ongoing simulations are also needed to explore methods of reducing bremsstrahlung losses in p+boron reactors, however reducing electron losses is the more important problem of the two.

In addition to the above problems with p+boron, the present design has a problem with ion injection. The boron ion guns simulated in this work were assumed to produce about 200mA of ion current. This level of current output is several orders of magnitude beyond the capability of existing ion guns, which typically produce microamps. An ion gun design capable of fueling at least a scale model p+boron reactor is needed before a net power reactor can be seriously contemplated.

To avoid the ion source issue and to focus on reducing the electron losses, it seems best to return to simulating D+D reactors. With D+D reactors the bremsstrahlung losses are negligible and the electron losses are the same or simply related to p+boron reactors. This plan would concentrate on solving the more important electron loss problem first.

Additional simulation of D+D reactors is also needed to compare with the WB-8 scale model reactor data accumulated by the EMC2 Corporation(http://www.emc2fusion.org/) over the past few years. As reported on the talk-polywell.org website, ref. [9] below, it appears that the U.S. Navy support for the EMC2 Corporation development may come to an end on 30 June, 2012. Hopefully the accumulated D+D test data, so far held in secret, will soon after be made public so comparison with these ongoing D+D simulations can be made. Data comparison is essential for refining the parameters of the simulation model.

[8] http://www.plasma.ee.kansai-u.ac.jp/iec2010/pdf/pdf_slides_posters/Rogers2.pdf

[9] http://talk-polywell.org/bb/viewtopic.php?t=1681&postdays=0&postorder=asc&start=900 then scroll down to "ladajo Posted: Tue Dec 13, 2011 7:27 pm"